FORECASTERS' FORUM

Introducing Lightning Threat Messaging Using the *GOES-16* Day Cloud Phase Distinction RGB Composite

CYNTHIA B. ELSENHEIMER

NOAA/NWS Southern Region Headquarters, Fort Worth, Texas

CHAD M. GRAVELLE[a]

Cooperative Institute for Mesoscale Meteorological Studies, University of Oklahoma, Norman, Oklahoma

(Manuscript received 9 March 2019, in final form 1 July 2019)

ABSTRACT

In 2001, the National Weather Service (NWS) began a Lightning Safety Awareness Campaign to reduce lightning-related fatalities in the United States. Although fatalities have decreased 41% since the campaign began, lightning still poses a significant threat to public safety as the majority of victims have little or no warning of cloud-to-ground lightning. This suggests it would be valuable to message the threat of lightning before it occurs, especially to NWS core partners that have the responsibility to protect large numbers of people. During the summer of 2018, a subset of forecasters from the Jacksonville, Florida, NWS Weather Forecast Office investigated if messaging the threat of cloud-to-ground (CG) lightning in developing convection was possible. Based on previous CG lightning forecasting research, forecasters incorporated new high-resolution *Geostationary Operational Environmental Satellite (GOES)-16* Day Cloud Phase Distinction red–green–blue (RGB) composite imagery with Multi-Radar Multi-Sensor isothermal reflectivity and total lightning data to determine if there was enough confidence to message the threat of CG lightning before it occurred. This paper will introduce the Day Cloud Phase Distinction RGB composite, show how it can add value for short-term lightning forecasting, and provide an operational example illustrating how fusing these datasets together may be able to provide confidence and extend the lead time when messaging the threat of cloud-to-ground lightning before it occurs.

1. Introduction

The National Weather Service (NWS) has recorded fatalities due to weather-related hazards in the United States since 1940 (https://www.weather.gov/hazstat/) and, based on total fatalities, lightning is the leading cause of deaths. Currently, the 10-yr average is 27 deaths annually, which is ranked seventh and behind the two leading causes of weather-related fatalities: heat (10-yr average of 101 annual fatalities) and flooding (10-yr average of 95 annual fatalities). When lightning fatalities are ranked by state, they occur most frequently in Florida and coincide with the highest cloud-to-ground (CG) lightning flash densities in the United States (e.g., Huffines and Orville 1999; Rudlosky and Fuelberg 2010; Holle et al. 2016). Between 2008 and 2018, 54 lightning fatalities occurred in Florida—more than twice the number in Texas, which was the second most during the same period. Although Florida is susceptible to lightning fatalities year-round, they occur most often during the warm season (June–August) when convection and lightning flash densities are greatest due to diabatic processes and the development of sea-breeze convergence zones (Hodanish et al. 1997).

Overall, lightning-related fatalities in the United States have decreased dramatically since the 1970s and dropped an additional 41% after 2001 when the NWS increased lightning public awareness through the NWS Lightning Safety Awareness Campaign (Jensenius 2016). This is likely due in part to the *"When Thunder Roars, Go Indoors"* slogan that was developed to mitigate the threat of lightning by encouraging people to take shelter at the first sign a

[a] Current affiliation: NOAA/NWS Southern Region Headquarters, Fort Worth, Texas.

Corresponding author: Cynthia B. Elsenheimer, cindy.elsenheimer@noaa.gov

DOI: 10.1175/WAF-D-19-0049.1

thunderstorm was approaching. However, Lengyel et al. (2005) state the majority (54%) of victims in lightning casualty cases they studied between 1995 and 2002 had little or no warning the threat of CG lightning was approaching. Therefore, it would be valuable to message the threat of lightning before it occurs and recent research has demonstrated short-term lightning forecasting skill.

To assist with short-term lightning forecasting, numerous studies have shown the applicability of a radar-based approach (e.g., Buechler and Goodman 1990). The foundation for these applied research studies is the noninductive graupel–ice collision thunderstorm charging theory (e.g., Takahashi 1978; Saunders et al. 2006). In the presence of supercooled liquid water within a convective updraft, noninductive charging exists when nonsticking collisions occur between graupel and smaller, upward moving ice crystals. Baker and Dash (1994) state when pieces of ice with different mass (i.e., ice crystal and graupel) are coated with a negatively charged quasi-liquid layer of water (i.e., supercooled liquid) and momentarily collide, the layer of water is responsible for the exchange of mass. The smaller ice crystal grows at a faster rate due to diffusion and charges positively. These collisions lead to an exchange of charge and storm-scale charge separation (e.g., Chylek et al. 2004; Petersen et al. 2005; Mosier et al. 2011). The result is the development of a strong electric field within the updraft and subsequent lightning (Zipser and Lutz 1994; Gremillion and Orville 1999). Therefore, the majority of short-term lightning forecasting research has been based on using radar data to identify the presence of graupel within the mixed-phase region (i.e., between −10° and −20°C) of a developing updraft. Studies such as Vincent et al. (2003), Wolf (2007), Mosier et al. (2011), and Seroka et al. (2012) used radar reflectivity thresholds at isothermal levels to objectively and statistically determine the best CG lightning forecast criteria. While the results from those studies are slightly different, the majority of recent radar-based research suggests using a 40-dBZ reflectivity threshold at the −10°C isotherm produces the best lightning forecasts in terms of the critical success index (Mosier et al. 2011). The Multi-Radar Multi-Sensor (MRMS) system, developed at the National Severe Storms Laboratory and the University of Oklahoma, provides operational isothermal radar reflectivity at the 0°, −10°, and −20°C levels using WSR-88D reflectivity and the vertical profile of environmental temperature from Rapid Refresh model analysis (Smith et al. 2016).

Dual-polarization (DP) radar observations provide the ability to identify hydrometers relevant to noninductive charging, such as graupel, hail, and supercooled raindrops (Woodard et al. 2012; Kumjian 2013). Studies such as Goodman et al. (1988), Jameson et al. (1996), and Bringi et al. (1997) used DP differential reflectivity Z_{DR} (≥0.5–1.0 dB) to identify columns of supercooled raindrops within the mixed phase of updrafts to anticipate initial lightning. In Woodard et al. (2012), Z_{DR} columns were used with horizontal isothermal reflectivity to investigate the initiation of total lightning in 31 thunderstorms and 19 nonthunderstorms across northern Alabama. When compared against the 40-dBZ threshold at the −10°C isotherm benchmark used in previous research, they found Z_{DR} (1.0 dB with 40 dBZ at −10°C) was effective at reducing false alarms but provided little advancement in lead time and did not significantly improve current operational reflectivity-based lightning prediction algorithms. These results were supported by Scott and Carey (2014) where only modest improvements when using DP observations were found. Although the Z_{DR} columns identified in Woodard et al. (2012) were found using quasi-horizontal cross sections, the most common approach is to use vertical cross sections through the storm's core. In an operational environment, using vertical cross sections are time consuming when interrogating multiple cells and integrating multiple datasets. Furthermore, horizontal cross sections can be challenging when using temperature thresholds because the height of radar bins increase away from the radar on constant elevation scans. To eliminate the difficulty with using horizontal cross sections, it is common for to compute and use isothermal Z or Z_{DR} (Schultz et al. 2013). However, isothermal Z_{DR} is not available to operational meteorologists at this time.

Intracloud (IC) lightning detections, from the National Lightning Detection Network (NLDN; Cummins and Murphy 2009) and Earth Networks Total Lightning Network (ENTL; Liu and Heckman 2012), have also been used for short-term CG lightning forecasting. The strong electric field that develops within a convective updraft often initiates IC lightning before CG lightning. Krehbiel (1986), and others, state this occurs because 1) the electric field above the negative charge region in an updraft is stronger than the electric field below, and 2) the critical electric field required for discharges is smaller at lower atmospheric pressure higher in the updraft. Furthermore, Bruning and MacGorman (2013) and Calhoun et al. (2013) formulated that high IC flash rates occur due to turbulent motions near the updraft core where noninductive charging from graupel–ice crystal collisions is favored. These reasons are why IC lightning tends to occur 5–10 times more often during the life cycle of a thunderstorm (Krehbiel 1986) and why IC lightning is directly correlated with

updraft intensity (e.g., Goodman et al. 2005; Tessendorf et al. 2005; Deierling and Petersen 2008; Gatlin and Goodman 2010). With the advent of IC lightning detections from the NLDN and ENTL, the research community has applied these datasets for short-term lightning forecasting. Holle et al. (2016) found using NLDN IC lightning as a precursor for the first CG lightning strike increased the probability of detection of subsequent CG strikes by 13% over just using CG lightning detections alone. After analyzing 13 years of Northern Alabama Lightning Mapping Array data around NASA's Marshall Space Flight Center, Schultz et al. (2017) found that IC lightning occurred before CG lightning 75% of the time with a median lead time of 8 min before the first CG lightning detections.

The launch of the first two satellites in the Geostationary Operational Environmental Satellite (GOES)-R series, *GOES-16* and *GOES-17*, has brought state-of-the-art detection of atmospheric threats courtesy of the Advanced Baseline Imager (ABI). In addition to the increases in spatial and temporal resolution, the ABI includes a 16-band radiometer, with 2 visible channels, 4 near-infrared channels, and 10 infrared (IR) channels (Schmit et al. 2005) that offer operational meteorologists new diagnostic capabilities. However, more information can be obtained quicker by combining several multispectral channels into a single red–green–blue (RGB) composite image. RGB composites are created by assigning specific spectral channels or channel differences to red (R), green (G), and blue (B) colors. When combined into a false color RGB composite, the image can be used as a decision aid to enhance specific meteorological features (Elmer et al. 2016; Fuell et al. 2016).

The *GOES-16/17* have given operational meteorologists in the Western Hemisphere the ability to observe the cloud-top dominant particle type and implied charge separation process in developing convection from a geostationary perspective for the first time. Although only operational for a little over a year, these capabilities may provide the opportunity to enhance short-term lightning forecasting and National Weather Service (NWS) Impact-based Decision Support Services (IDSS). Therefore, the purpose of this operationally relevant forecaster's forum article is twofold: to introduce how the Day Cloud Phase Distinction (DCPD) RGB composite can be used for short-term forecasting of initial CG lightning when integrated with MRMS and total lightning data, and to show how this information can be used to message the threat of lightning before it occurs to enhance the IDSS provided to NWS core partners.

2. Day Cloud Phase Distinction RGB composite

The DCPD RGB composite is created by using

$$(\mathrm{R},\mathrm{G},\mathrm{B}) = 255\left[\frac{(\mathrm{TB},\,\Delta\mathrm{TB},\,R,\,\Delta R) - \mathrm{MIN}}{\mathrm{MAX} - \mathrm{MIN}}\right]^{(1/\gamma_{\mathrm{R,G,B}})}, \quad (1)$$

where (TB, ΔTB, R, ΔR) is the brightness temperature (BT), brightness temperature difference (BTD), reflectance, or reflectance difference, respectively; MAX is the upper threshold value; MIN is the lower threshold value; and γ is the gamma enhancement value (EUMETSAT 2009; Zavodsky et al. 2013; Elmer et al. 2016; Fuell et al. 2016). The DCPD RGB uses the following three GOES-R spectral bands: 10.35 μm (clean infrared), 0.64 μm (red visible), and 1.61 μm (snow/ice). The red component of the DCPD RGB uses the inverse of the 10.35-μm BT ranging from 7.5° to −53.5°C to indicate surface and cloud-top BTs. A small red component pixel contribution (warm BT) indicates sensing warm land, warm water, or low clouds and a large red component pixel contribution (cold BT) indicates cold land, high clouds, or snow. The green component uses the 0.64-μm reflectance ranging from 0% to 78% and physically relates to the reflectance of clouds, land, and water surfaces. Therefore, the green component can distinguish between highly reflective surfaces (large green contribution) such as clouds, snow, and white sand and surfaces with lower reflectance (small green contribution) such as water and vegetative land. The blue component uses the 1.61-μm reflectance ranging from 0% to 59% to indicate the particle phase of a pixel. A large contribution from the blue component indicates a highly reflective surface (e.g., liquid clouds) and a small contribution indicates poorly reflective surfaces (e.g., ice clouds).

After combining the RGB color components, an example of the DCPD RGB composite false color image from 21 March 2018 is shown in Fig. 1. When interpreting RGB composites, it is important to remember colors physically relate to cloud microphysics, atmospheric features, and/or land features. In the DCPD RGB composite example, the following are present: low-level liquid clouds (cyan), midlevel liquid clouds (lavender), glaciating clouds (green/yellow; i.e., mixed-phase cloud), thin upper-level ice clouds (orange), thick upper-level ice clouds (yellow), and snow/ice (green). This example illustrates one of the strengths of the DCPD RGB composite when compared to 0.64- or 10.35-μm single-band imagery: the ability to quickly identify different cloud layers and phases. For example, in the DCPD RGB composite thick upper-level

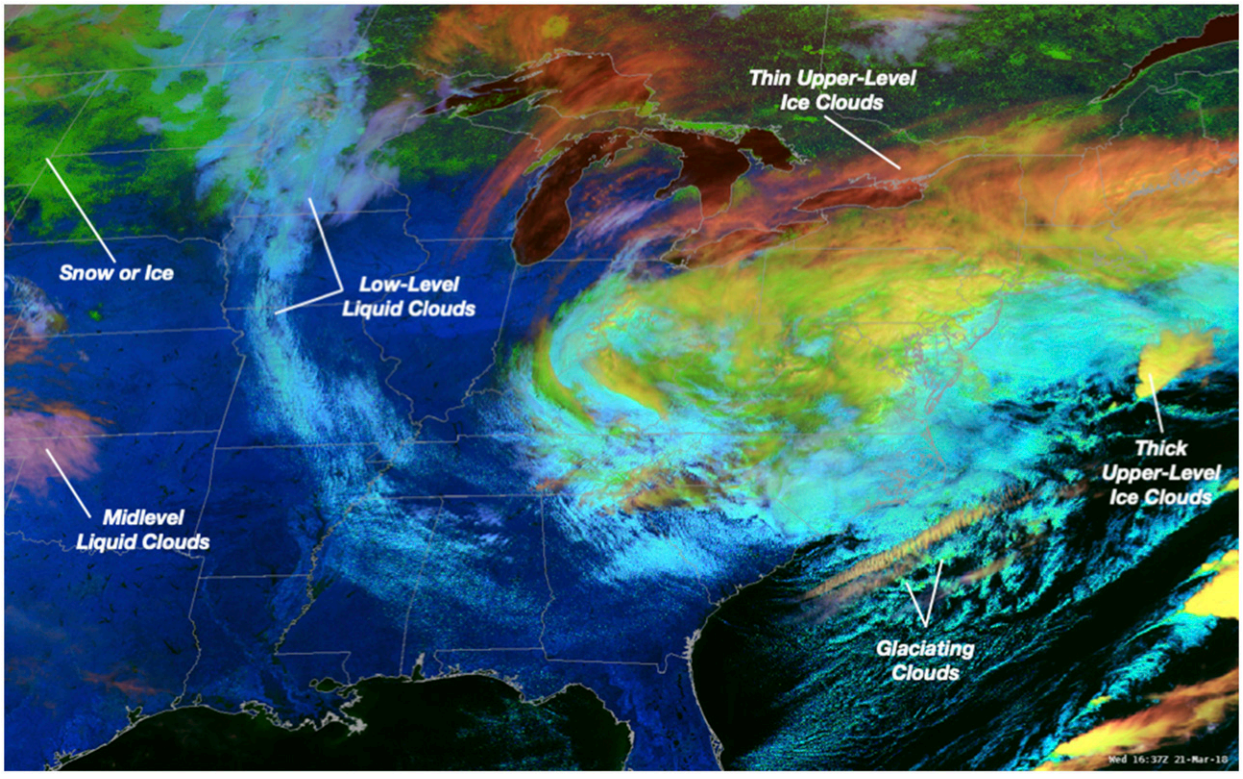

FIG. 1. Example of the *GOES-16* Day Cloud Phase Distinction RGB composite valid at 1637 UTC 21 Mar 2018 illustrating cloud layers, cloud types, snow, and ice.

ice clouds are yellow because there are large red (cold BT) and green component (highly reflective clouds) contributions with a small blue component (lower reflective ice clouds) contribution. Another strength of the DCPD RGB composite is the ability to easily differentiate snow from clouds, which can be important for short-term temperature forecasts. This is illustrated in Fig. 1 across the northern plains and Northern Mississippi Valley where snow cover and low-level liquid clouds are adjacent. Snow is green because there is a large green component (highly reflective) contribution with small red (warm BT) and blue component (low reflectance) contributions.

In developing convection, previous research has shown the value of using the legacy 3.9-μm (shortwave infrared) and 10.7-μm (longwave infrared) GOES bands for initial lightning forecasting (e.g., Harris et al. 2010; Mecikalski et al. 2013). The legacy 10.7-μm band and its time trend are proxies for cloud-top cooling and can discriminate between immature and mature cumulus clouds (Mecikalski and Bedka 2006). The 3.9-μm reflectance infers cumulus clouds with significant updrafts that are glaciating at cloud top, an indicator of ongoing noninductive charging (Mecikalski et al. 2013). In the GOES-R era, the DCPD RGB composite can be used for observing cloud growth and dominant cloud-top particle type. As a cumulus cloud grows vertically into agitated cumulus to towering cumulus before becoming a mature cumulonimbus with IC and/or CG lightning, the particle type at the top of the cloud changes from liquid to mixed phase (i.e., liquid, supercooled liquid, and ice crystals) to predominantly ice crystals (Chylek et al. 2004 and illustrated in Fig. 2). The result in the DCPD RGB composite is a vertically developing convective updraft that changes from cyan to green/yellow (comparing *GOES-16* inset in Figs. 2a and 2c). The reason for the change in the DCPD RGB composite is twofold. First, as the updraft grows vertically the cloud-top temperature associated with the 10.35-μm spectral band (10.7-μm brightness temperature in legacy GOES) decreases and the red contribution to the RGB composite increases. Second, as ice crystals reach the top of the updraft, both reflectance in the 1.61-μm spectral band (3.9-μm reflectance in legacy GOES) and the blue contribution to the RGB composite decrease. This is shown in the *GOES-16* DCPD RGB composite example in Fig. 2, where the percent of the red component increases from 18% to 57% (based on color saturation of 100%) and the percent of the blue component decreases

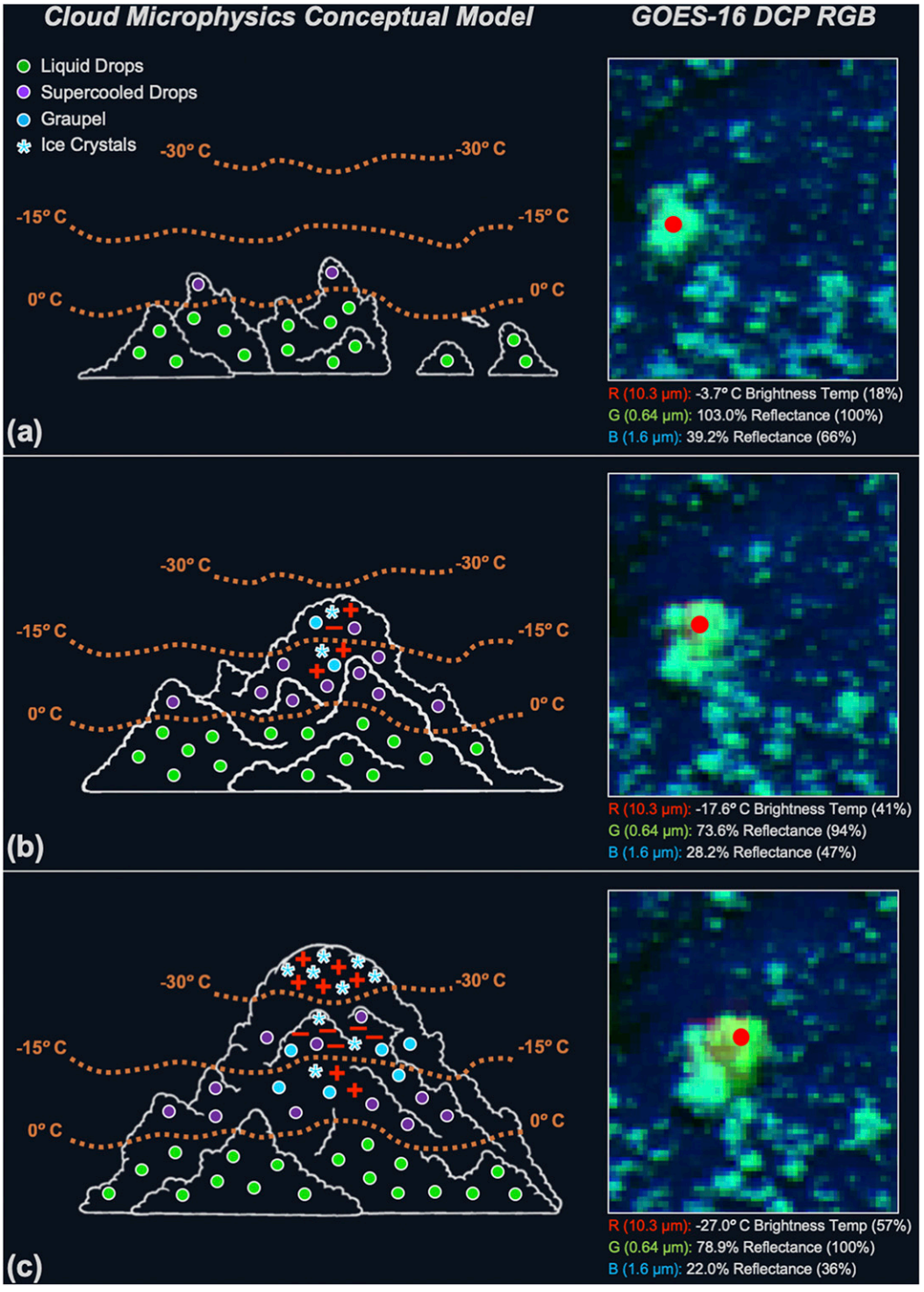

FIG. 2. Conceptual model and associated *GOES-16* Day Cloud Phase Distinction RGB composite illustrating the transition of (a) mostly liquid cumulus, (b) supercooled towering cumulus, (c) and mixed-phase towering cumulus as charge separation occurs due to noninductive charging theory. Isotherms in the conceptual model highlight key temperature thresholds important for observing the cloud-top phase change during charge separation, red positive and negative symbols depict the electric charge distribution in a typical thunderstorm, and the red circle in each *GOES-16* Day Cloud Phase Distinction RGB composite inset is the location where red, green, and blue component single band values and percentage of color saturation (0%–100%) were observed.

from 66% to 36%. Finally, since cumulus, towering cumulus, and cumulonimbus clouds are highly reflective, the 0.64-μm spectral band reflectance and green contribution to the RGB composite are both large as a convective updraft intensifies. Therefore, the green component does not tend to fluctuate in developing convection. The main limitations in using the DCPD RGB composite to monitor the cloud-top phase change are that it is a daytime only application, low solar angles impact the reflectance values of 0.64 and 1.61 μm near sunrise and sunset, and deep convection with dense cirrus overcast (e.g., associated with mature squall lines and mesoscale convective systems) can obscure the development of new convection.

3. Messaging the threat of lightning—An operational example

To leverage and exploit the increase in lead time for lightning initiation by using radar and geostationary satellite data together, as suggested by Mecikalski et al. 2013, an operational example is presented that shows how integrating the DCPD RGB composite, MRMS isothermal reflectivity, and total lightning data can allow for the anticipatory communication of CG lightning threats to NWS core partners. During the summer of 2018, as a proof of concept, a subset of forecasters from the NWS Weather Forecast Office (WFO) in Jacksonville, Florida, attempted to message the threat of CG lightning in developing convection before it occurred. Since an official NWS lightning product does not exist, forecasters used Twitter to disseminate lightning threat messages while monitoring developing convective updrafts in populated areas. When forecasters were confident a liquid to mixed-phase transition was occurring in the DCPD RGB composite, MRMS isothermal reflectivity suggested graupel was developing in the updraft, and charge separation was imminent, a tweet would be sent stating the threat of lightning was increasing over the next 15–30 min. The following is an operational example that highlights how NWS Jacksonville forecasters used the *GOES-16* DCPD RGB composite, MRMS isothermal reflectivity, and ENTL data to message the threat of CG lightning to core partners and the general public.

At 1500 UTC 21 June 2018, a weak surface trough was analyzed in surface observations and *GOES-16* CONUS (i.e., 5-min temporal cadence) satellite imagery moving southeastward across northeast Florida (Fig. 3, top). Ahead of the surface trough, showers and thunderstorms were ongoing southwest of Ocala, Florida, and towering cumulus were developing eastward to Daytona Beach, Florida. Behind the trough, northwest flow prevailed and by 1632 UTC a cumulus field was developing inland across Clay and Putnam Counties and along the sea breeze boundary across St. Johns and Flagler Counties (Fig. 3, bottom). Along the East Coast sea breeze, under large-scale westerly and northwesterly flow, initial deep convection often develops when the upward branch of the sea breeze circulation is anchored along the coast. Therefore, convection can be more common near the beaches and northeast Florida beachgoers are more susceptible to the threat of lightning if convection develops.

At 1642 UTC, NWS Jacksonville forecasters were monitoring towering cumulus that developed along the Clay and Putnam county line (Fig. 4a) and by 1702 UTC a dominant updraft was visible in both the DCPD RGB composite and MRMS −10°C isothermal reflectivity in far northeastern Putnam County (Fig. 4b). In the *GOES-16* DCPD RGB composite, cloud tops were cyan (i.e., mostly liquid) and MRMS reflectivity was ~30 dBZ within the updraft. Ten minutes later, at 1712 UTC, the updraft continued to strengthen and the DCPD RGB composite and MRMS data suggested charge separation had begun (Fig. 4c). Graupel was likely present in the updraft as >40 dBZ was observed in MRMS −10°C isothermal reflectivity data. Additionally, the DCPD RGB composite provided confidence that charge separation was taking place as small ice crystals began to reach the top of the updraft, depicted by the green/yellow cloud tops. The change in the DCPD RGB composite appearance can be shown quantitatively by examining the evolution of each component's color saturation when sampled at the top of the updraft (Fig. 5). Between 1702 and 1707 UTC, the contribution of the RGB composite's blue component (i.e., 1.61-μm reflectance) decreased from 66% to 35% due to a decrease in reflectance from 38.9% to 20.4% as ice crystals became the dominant particle type at the top of the updraft. As the updraft grew, cloud-top temperature cooled from −3.1° to −22.2°C between 1707 and 1712 UTC and the contribution of the RGB composite's red component increased from 17% to 49%. These physical changes at the top of the updraft are responsible for the evolution of hue from cyan to green/yellow in the DCPD RGB composite. Using MRMS isothermal reflectivity and a basic understanding of noninductive charge theory as visualized via the DCPD RGB composite, the forecaster monitoring the developing convection became confident that IC and CG lightning were imminent. At 1717 UTC the first ENTL IC lightning occurred, and at 1721 UTC the first ENTL CG lightning was observed; approximately 12 min after charge separation was implied in the DCPD RGB composite.

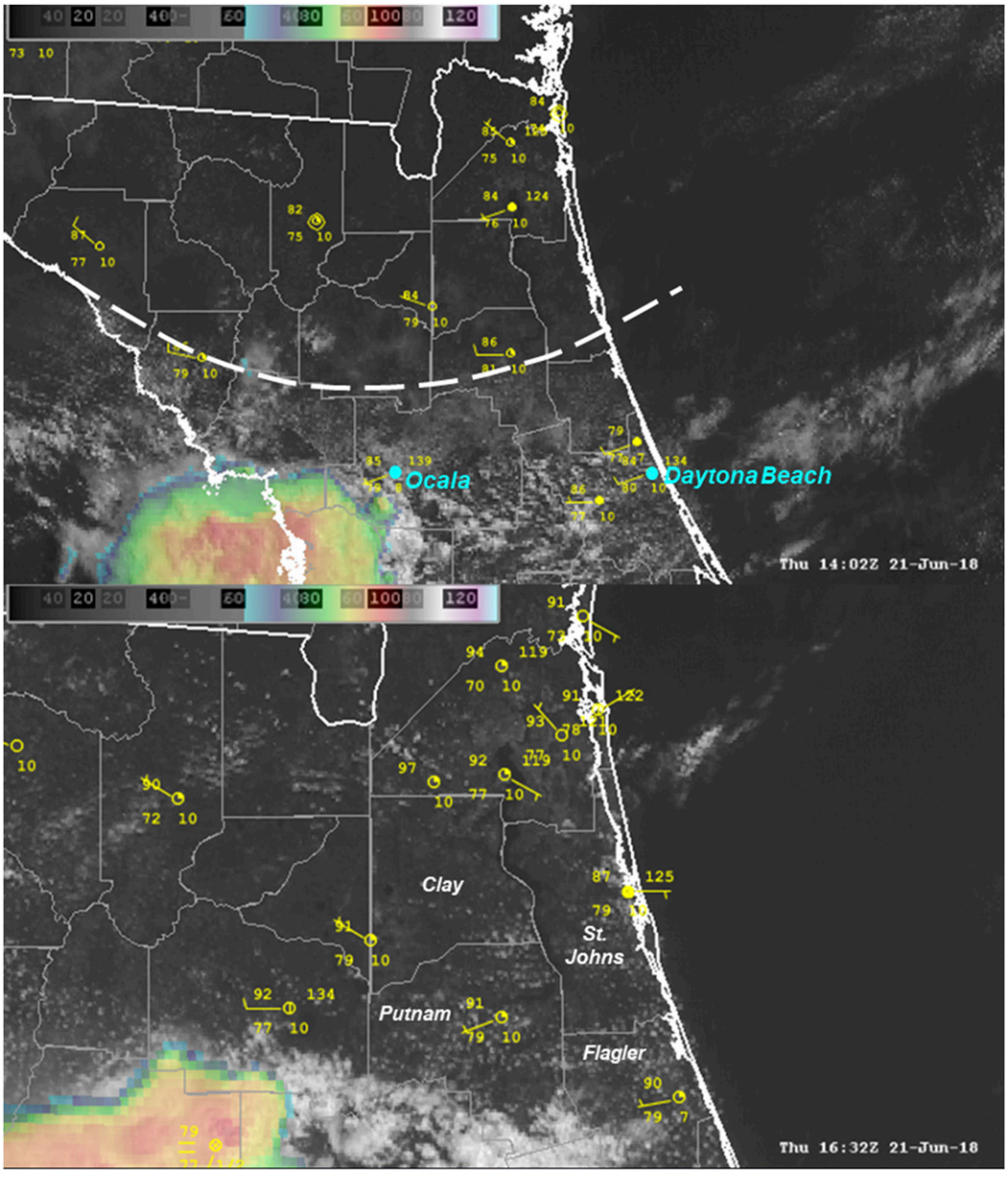

FIG. 3. (top) *GOES-16* 0.64- and 10.35-μm merged imagery with surface observations valid at 1402 UTC 21 Jun 2018 over the northern Florida peninsula. The white dashed line indicates the subjective location of the surface trough. (bottom) As in the top panel, but for the northeast Florida peninsula and valid at 1632 UTC. Florida counties of Clay, St. Johns, Putnam, and Flagler are labeled.

Because this thunderstorm was developing in rural Putnam County, a lightning threat message was not posted to Twitter.

While convective initiation was occurring in Putnam County, at 1702 UTC along the beaches of St. Johns County, towering cumulus was developing in the *GOES-16* DCPD composite along the sea breeze boundary from Vilano Beach to St. Augustine Beach, Florida (Fig. 6a). At this time, the cloud tops of the towering cumulus were cyan and exhibiting slow, steady growth. By 1717 UTC, two dominant towers were evident in *GOES-16* imagery and MRMS −10°C isothermal reflectivity; one just west of Vilano Beach and one just west of St. Augustine Beach (Fig. 6b). Five minutes later, at 1722 UTC, the DCPD RGB composite transitioned to green/yellow just west of St. Augustine, indicating ice crystals had begun to reach the top of that convective tower (Fig. 6c). This is

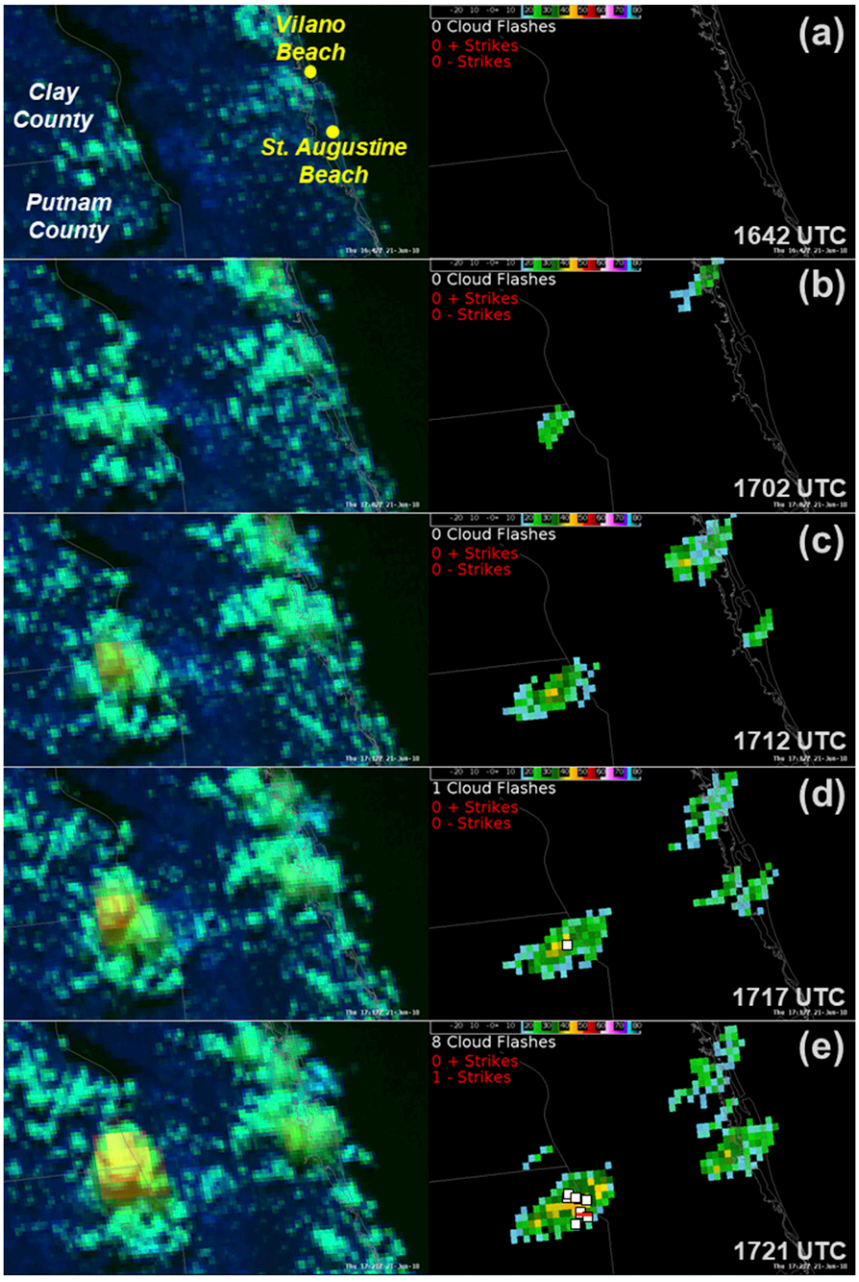

FIG. 4. (a)–(e) *GOES-16* Day Cloud Phase Distinction RGB composite on the left and MRMS −10°C isothermal reflectivity (dB*Z*; shaded according to scale) with ENTL IC (white squares) and ENTL CG (red positive and negative symbols) lightning observations on the right valid at (a) 1642, (b) 1702, (c) 1712, (d) 1717, and (e) 1721 UTC 21 Jun 2018.

due to the contribution of the DCPD RGB composite blue component decreasing from 68% to 39% as 1.61-μm reflectance decreased from 40.1% to 23.3% (Fig. 7). Based on the implied charge separation in the DCPD RGB composite and defined vertical growth over the last 20 min, NWS Jacksonville forecasters were confident enough to message the threat of lightning at 1724 UTC for vulnerable beachgoers at Vilano Beach and St. Augustine Beach (Fig. 8). Over the next five minutes, the updraft continued to intensify. At 1729 UTC, a well-defined 40-dB*Z* echo was apparent in MRMS −10°C isothermal reflectivity just west of St. Augustine Beach and the first IC lightning was observed in ENTL data (Fig. 6d). At 1733 UTC, the first CG

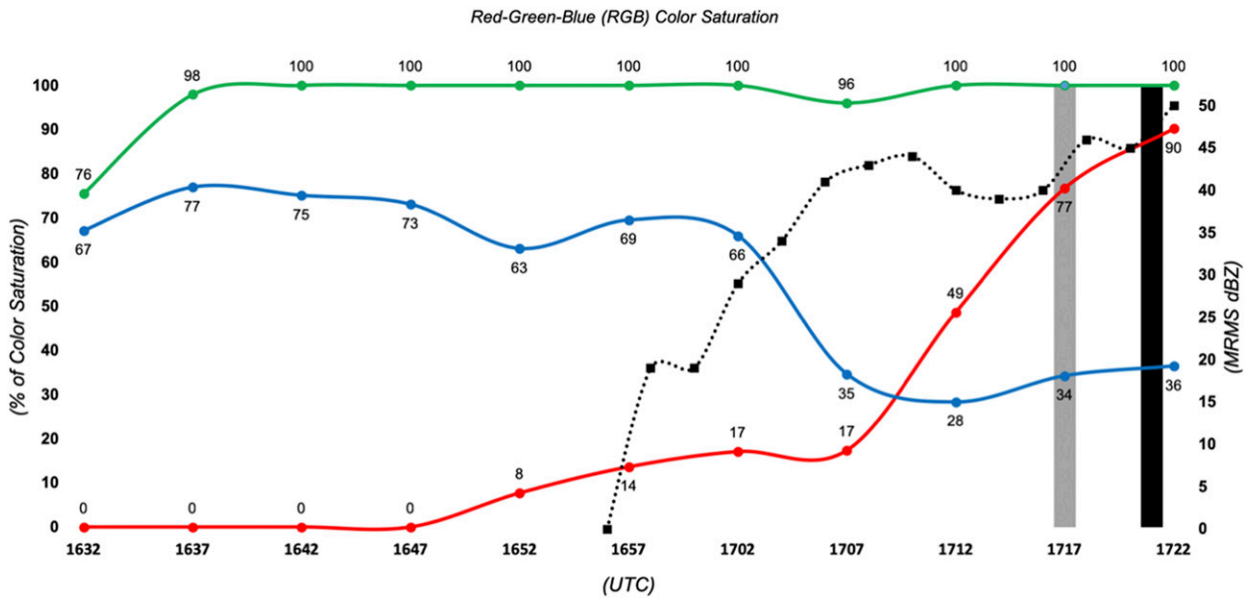

FIG. 5. Putnam County storm time series of *GOES-16* Day Cloud Phase Distinction RGB composite red component color saturation (%; red solid trace), green component color saturation (%; green solid trace), and blue component color saturation (%; blue solid trace), MRMS −10°C isothermal reflectivity (dB*Z*; black dotted trace), initial ENTL in-cloud lightning (vertical gray bar), and initial ENTL cloud-to-ground lightning (vertical black bar) between 1632 and 1722 UTC 21 Jun 2018.

lightning occurred one-quarter mile southwest of St. Augustine Beach (Fig. 6e); 9 min after the initial lightning threat tweet was sent.

These two examples demonstrate how the DCPD RGB composite strengthens the short-term CG lightning forecasting conceptual model. The DCPD RGB provides forecasters the ability, in real time, to monitor the cloud-top phase change of developing cumulonimbus clouds at high temporal and spatial resolution with low latency; a capability not possible with legacy *GOES-13/14/15* data (Gravelle et al. 2016). Integrating this satellite imagery may provide the forecaster with the confidence to forecast, rather than hindcast, the threat of lightning when requested for IDSS.

4. Discussion

The purpose of this forecaster's forum article was to introduce the *GOES-16* DCPD RGB composite to operational forecasters and demonstrate how using that imagery with MRMS isothermal reflectivity and total lightning data can provide confidence when messaging the threat of initial CG lightning in developing convection. Using this approach, between 1 June and 1 August 2018, a subset of NWS Jacksonville forecasters messaged the threat of lightning 45 unique times before it occurred. As in the example presented from 21 June 2018, the messaging was targeted to vulnerable populations (i.e., those possibly participating in outdoor leisure activities in populated areas) in the Jacksonville, Gainesville, and St. Augustine, Florida, areas, along the beaches of northeast Florida and southeast Georgia, and along the St. Johns River.

While Twitter was the arena for the lightning threat messages, disseminating lightning threats publicly was never the end goal. In geographic areas where convection and associated lightning threats are common, such as in locations that frequently experience pulse and sea breeze convection, messaging the threat of lightning for every thunderstorm is neither feasible nor warranted. Instead, working with NWS core partners to determine their needs within an IDSS framework can result in a more meaningful approach to lightning threat information. Coordinating critical timing thresholds with public safety officials to provide them lightning messaging when thunderstorms are developing near outdoor events or venues, such as outdoor sporting events or public beaches, is achievable. For example, on 3 August 2018 NWS Jacksonville forecasters were providing remote IDSS and lightning threat messages to law enforcement facilitating an active shooter drill at a local high school. Using the *GOES-16* DCPD RGB composite, MRMS isothermal reflectivity data, and total lightning data, forecasters alerted law enforcement that CG lightning was possible 34 min before the first CG lightning occurred. In this case, forecasters provided the IDSS to law enforcement through a phone call. However, a more efficient dissemination method

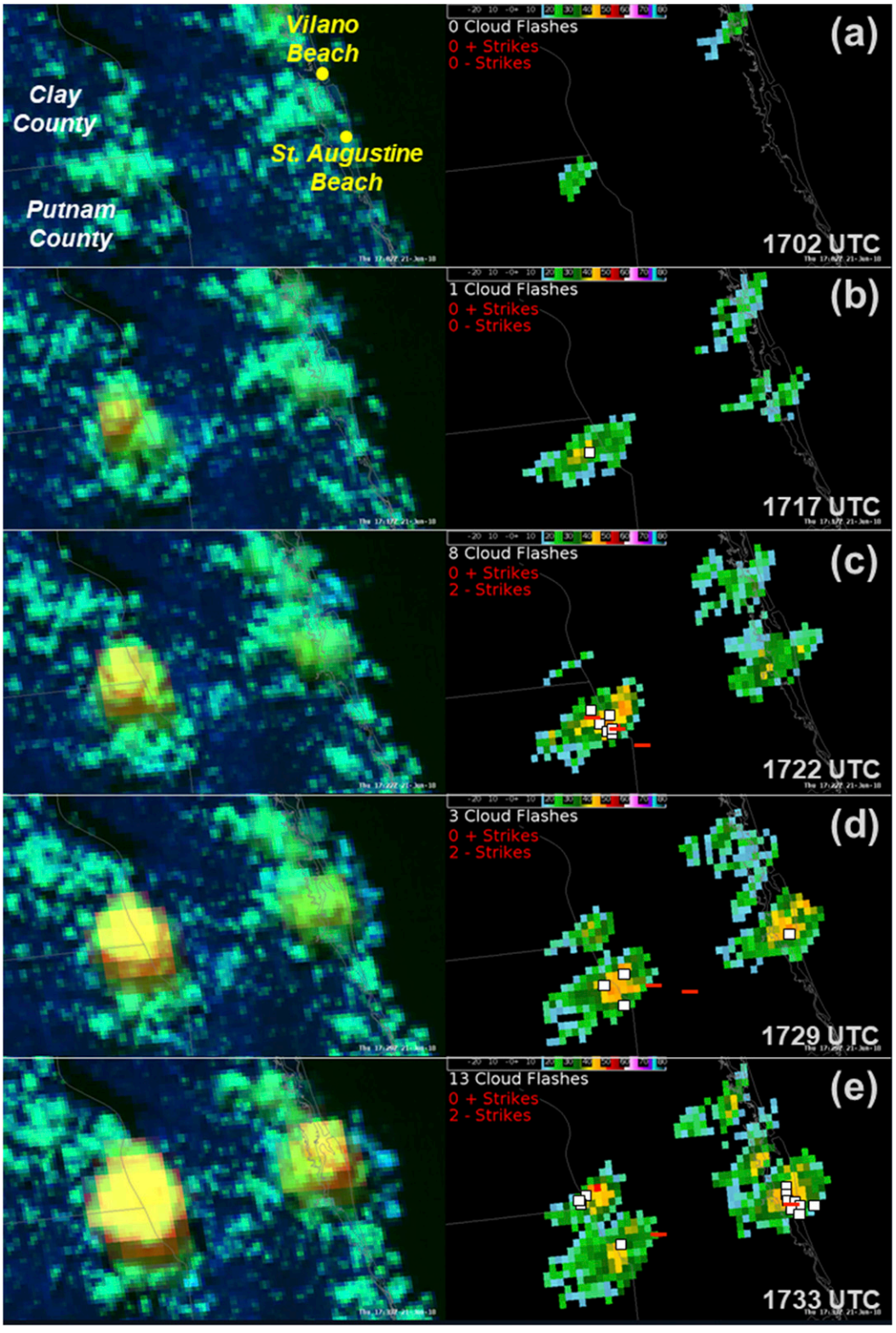

FIG. 6. (a)–(e) *GOES-16* Day Cloud Phase Distinction RGB composite on the left and MRMS −10°C isothermal reflectivity (dB*Z*; shaded according to scale) with ENTL IC (white squares) and ENTL CG (red positive and negative symbols) lightning observations on the right valid at (a) 1702, (b) 1717, (c) 1722, (d) 1729, and (e) 1733 UTC 21 Jun 2018.

FIG. 7. St. Augustine storm time series of *GOES-16* Day Cloud Phase Distinction RGB composite red component color saturation (%; red solid trace), green component color saturation (%; green solid trace), and blue component color saturation (%; blue solid trace), MRMS −10°C isothermal reflectivity (dBZ; black dotted trace), initial ENTL in-cloud lightning (vertical gray bar), and initial ENTL cloud-to-ground lightning (vertical black bar) between 1647 and 1737 UTC 21 Jun 2018.

may be to use a modified version of the wildfire notification tool developed by the NWS WFO in Norman, Oklahoma (Lindley et al. 2016). The notification tool can be integrated within the NWS Advanced Weather Interactive Processing System to efficiently communicate lightning threat information and IDSS to core partners that need to make quick public safety decisions.

During the NWS Jacksonville proof of concept, forecasters gained confidence with integrating the discussed datasets to message the threat of lightning before it occurred in predominately sea-breeze convection regimes with weakly forced, isolated convection. Although verification metrics and lead time statistics are essential in determining the added value of incorporating the DCPD RGB with other short-term lightning forecasting methods, they can be resource intensive outside the research community and are beyond the scope of this publication. One method to address this challenge would be to determine and document when rapid changes occur in the blue and red

FIG. 8. (left) NWS Jacksonville WFO tweet sent at 1724 UTC 21 Jun 2018 messaging the threat of CG lightning near St. Augustine Beach and Vilano Beach. (right) NWS Jacksonville WFO tweet sent at 1736 UTC 21 Jun 2018 messaging the occurrence of cloud-to-ground lightning at St. Augustine Beach.

components of the DCPD RGB as the convective updraft intensifies, as shown in Figs. 5 and 7. Occasionally, there were times when charge separation was implied in the DCPD RGB composite but the result was orphan anvils (Gravelle et al. 2016; Line et al. 2016) that did not produce IC or CG lightning. Within a near-tropical environment driven by mesoscale forcing, these convective initiation "failures" in the DCPD RGB could be the result of weak inhibition where early attempts at deep moist convection occur before the sea-breeze circulation develops. The result is numerous scattered showers within weak updrafts that lack the graupel necessary to initiate the noninductive charging process (Fig. 2a and Bringi et al. 1997). While false alarms were not common, their occurrence suggests the need for robust applied climatological research using these tools for short-term lightning prediction. As discussed in section 1, the short-term CG lightning prediction studies in the literature have focused on using individual datasets (e.g., isothermal radar reflectivity or total lightning data). To provide the most applicable results to the operational community, it is critical that future verification research integrates *GOES-16*, MRMS, and total lightning data from ground-based and satellite-based sensors. Not only would these results provide integrated verification metrics, they would assist NWS forecasters with communicating the limits of predictability of CG lightning at specific lead times to core partners. In addition to understanding verification statistics, it is important for operational forecasters to continue to apply new technology and guidance to short-term lightning forecasting. For example, including machine learning short-term lightning probabilistic guidance that uses big data (Meyer et al. 2016; Calhoun et al. 2018) into this process may allow NWS forecasters to message the threat of CG lightning even better in the next few years.

Acknowledgments. The authors thank Kim Runk (NOAA/NWS Operations Proving Ground), Matthew Foster (NOAA/NWS Operations Proving Ground), and JJ Brost (NOAA/NWS Southern Region Headquarters) for their reviews of earlier versions of this manuscript. We also thank the staff at the NOAA/NWS Forecast Office at Jacksonville, FL, NOAA/NWS Southern Region Headquarters, and NOAA/NWS Operations Proving Ground for their support with this project. Finally, thank you to the four anonymous reviewers for their helpful feedback that improved this publication. Funding was provided by NOAA/Office of Oceanic and Atmospheric Research under NOAA-University of Oklahoma Cooperative Agreement NA16OAR4320115, U.S. Department of Commerce.

REFERENCES

Baker, M. B., and J. G. Dash, 1994: Mechanism of charge transfer between colliding ice particles in thunderstorms. *J. Geophys. Res.*, **99**, 10 621–10 626, https://doi.org/10.1029/93JD01633.

Bringi, V. N., K. Knupp, A. Detwiler, L. Liu, I. J. Caylor, and R. A. Black, 1997: Evolution of a Florida thunderstorm during the Convection and Precipitation/Electrification Experiment: The case of 9 August 1991. *Mon. Wea. Rev.*, **125**, 2131–2160, https://doi.org/10.1175/1520-0493(1997)125<2131:EOAFTD>2.0.CO;2.

Bruning, E. C., and D. R. MacGorman, 2013: Theory and observations of controls on lightning flash size spectra. *J. Atmos. Sci.*, **70**, 4012–4029, https://doi.org/10.1175/JAS-D-12-0289.1.

Buechler, D. E., and S. J. Goodman, 1990: Echo size and asymmetry: Impact on NEXRAD storm identification. *J. Appl. Meteor.*, **29**, 962–969, https://doi.org/10.1175/1520-0450(1990)029<0962:ESAAIO>2.0.CO;2.

Calhoun, K. M., D. R. MacGorman, C. L. Ziegler, and M. I. Biggerstaff, 2013: Evolution of lightning activity and storm charge relative to dual-Doppler analysis of a high-precipitation supercell storm. *Mon. Wea. Rev.*, **141**, 2199–2223, https://doi.org/10.1175/MWR-D-12-00258.1.

——, and Coauthors, 2018: Cloud-to-ground lightning probabilities and warnings within an integrated warning team. *Special Symp. on Impact-Based Decision Support Services*, Austin, TX, Amer. Meteor. Soc., 4.4, https://ams.confex.com/ams/98Annual/webprogram/Paper329888.html.

Chylek, P., C. C. Borel, and J. Klett, 2004: Mixed phase clouds, cloud electrification and remote sensing. Preprints, *Los Alamos Workshop on Lightning Monitoring from Space*, Santa Fe, NM, Los Alamos National Laboratory, 1–7.

Cummins, K. L., and M. J. Murphy, 2009: An overview of lightning locating systems: History, techniques, and data uses, with an in-depth look at the U.S. NLDN. *IEEE Trans. Electromagn. Compat.*, **51**, 499–518, https://doi.org/10.1109/TEMC.2009.2023450.

Deierling, W., and W. A. Petersen, 2008: Total lightning activity as an indicator of updraft characteristics. *J. Geophys. Res.*, **113**, D16210, https://doi.org/10.1029/2007JD009598.

Elmer, N. J., E. Berndt, and G. J. Jedlovec, 2016: Limb correction of MODIS and VIIRS infrared channels for the improved interpretation of RGB composites. *J. Atmos. Oceanic Technol.*, **33**, 1073–1087, https://doi.org/10.1175/JTECH-D-15-0245.1.

EUMETSAT, 2009: Best practices for RGB compositing of multi-spectral imagery. User Services Division, EUMETSAT, 8 pp., http://oiswww.eumetsat.int/~idds/html/doc/best_practices.pdf.

Fuell, K. K., B. J. Guyer, D. Kann, A. L. Molthan, and N. Elmer, 2016: Next generation satellite RGB dust imagery leads to operational changes at NWS Albuquerque. *J. Oper. Meteor.*, **4**, 75–91, https://doi.org/10.15191/nwajom.2016.0406.

Gatlin, P. N., and S. J. Goodman, 2010: A total lightning trending algorithm to identify severe thunderstorms. *J. Atmos. Oceanic Technol.*, **27**, 3–22, https://doi.org/10.1175/2009JTECHA1286.1.

Goodman, S. J., D. E. Buechler, P. D. Wright, and W. D. Rust, 1988: Lightning and precipitation history of a microburst-producing storm. *Geophys. Res. Lett.*, **15**, 1185–1188, https://doi.org/10.1029/GL015i011p01185.

——, and Coauthors, 2005: The North Alabama Lightning Mapping Array: Recent severe storm observations and future prospects. *Atmos. Res.*, **76**, 423–437, https://doi.org/10.1016/j.atmosres.2004.11.035.

Gravelle, C. M., K. J. Runk, K. L. Crandall, and D. W. Snyder, 2016: Forecaster evaluations of high temporal satellite imagery for the GOES-R era at the NWS Operations Proving Ground. *Wea. Forecasting*, **31**, 1157–1177, https://doi.org/10.1175/WAF-D-15-0133.1.

Gremillion, M. S., and R. E. Orville, 1999: Thunderstorm characteristics of cloud-to-ground lightning at the Kennedy Space Center, Florida: A study of lightning initiation signatures as indicated by the WSR-88D. *Wea. Forecasting*, **14**, 640–649, https://doi.org/10.1175/1520-0434(1999)014<0640:TCOCTG>2.0.CO;2.

Harris, R. J., J. R. Mecikalski, W. M. MacKenzie Jr., P. A. Durkee, and K. E. Nielsen, 2010: The definition of GOES infrared lightning initiation interest fields. *J. Appl. Meteor. Climatol.*, **49**, 2527–2543, https://doi.org/10.1175/2010JAMC2575.1.

Hodanish, S., D. Sharp, W. Collins, C. Paxton, and R. E. Orville, 1997: A 10-yr monthly lightning climatology of Florida: 1986–95. *Wea. Forecasting*, **12**, 439–448, https://doi.org/10.1175/1520-0434(1997)012<0439:AYMLCO>2.0.CO;2.

Holle, R. L., K. L. Cummins, and W. A. Brooks, 2016: Seasonal, monthly, and weekly distributions of NLDN and GLD360 cloud-to-ground lightning. *Mon. Wea. Rev.*, **144**, 2855–2870, https://doi.org/10.1175/MWR-D-16-0051.1.

Huffines, G. R., and R. E. Orville, 1999: Lightning ground flash density and thunderstorm duration in the continental United States: 1989–96. *J. Appl. Meteor.*, **38**, 1013–1019, https://doi.org/10.1175/1520-0450(1999)038<1013:LGFDAT>2.0.CO;2.

Jameson, A. R., M. J. Murphy, and E. P. Krider, 1996: Multiple-parameter radar observations of isolated Florida thunderstorms during the onset of electrification. *J. Appl. Meteor.*, **35**, 343–354, https://doi.org/10.1175/1520-0450(1996)035<0343:MPROOI>2.0.CO;2.

Jensenius, J. S., 2016: NOAA's lightning safety awareness efforts—What we've accomplished in 15 years. Preprints, *24th Int. Lightning Detection Conf. and Sixth Int. Lightning Meteorology Conf.*, San Diego, CA, Vaisala, 1–5.

Krehbiel, P. R., 1986: The electrical structure of thunderstorms. *The Earth's Electrical Environment*, E. P. Krider and R. G. Roble, Eds., National Academy Press, 90–113.

Kumjian, M. R., 2013: Principles and applications of dual-polarization weather radar. Part I: Description of the polarimetric radar variables. *J. Oper. Meteor.*, **1**, 226–242, https://doi.org/10.15191/nwajom.2013.0119.

Lengyel, M. M., H. E. Brooks, R. L. Holle, and M. A. Cooper, 2005: Lightning casualties and their proximity to surrounding cloud-to-ground lightning. *14th Symp. on Education*, San Diego, CA, Amer. Meteor. Soc., P1.35, http://ams.confex.com/ams/pdfpapers/85775.pdf.

Lindley, T. T., A. R. Anderson, V. N. Mahale, T. S. Curl, W. E. Line, S. S. Lindstrom, and A. S. Bachmeier, 2016: Wildfire detection notifications for impact-based decision support services in Oklahoma using geostationary super rapid scan satellite imagery. *J. Oper. Meteor.*, **4**, 182–191, https://doi.org/10.15191/nwajom.2016.0414.

Line, W. E., T. J. Schmit, and S. J. Goodman, 2016: Use of geostationary super rapid scan satellite imagery by the Storm Prediction Center. *Wea. Forecasting*, **31**, 483–494, https://doi.org/10.1175/WAF-D-15-0135.1.

Liu, C., and S. Heckman, 2012: Total lightning data and real-time severe storm prediction. *TECO-2012—WMO Tech. Conf. on Meteorological and Environmental Instruments and Methods of Observation*, Brussels, Belgium, World Meteorological Organization, P5(10).

Mecikalski, J. R., and K. M. Bedka, 2006: Forecasting convective initiation by monitoring the evolution of moving cumulus in daytime GOES imagery. *Mon. Wea. Rev.*, **134**, 49–78, https://doi.org/10.1175/MWR3062.1.

——, X. Li, L. D. Carey, E. W. McCaul Jr., and T. A. Coleman, 2013: Regional comparison of GOES cloud-top properties and radar characteristics in advance of first-flash lightning initiation. *Mon. Wea. Rev.*, **141**, 55–74, https://doi.org/10.1175/MWR-D-12-00120.1.

Meyer, T. C., K. M. Kuhlman, D. M. Kingfield, and D. J. Gagne II, 2016: Using random forest technique to create cloud-to-ground lightning probabilities. *28th Conf. on Severe Local Storms*, Portland, OR, Amer. Meteor. Soc., 146, https://ams.confex.com/ams/28SLS/webprogram/Paper301841.html.

Mosier, R. M., C. Schumacher, R. E. Orville, and L. D. Carey, 2011: Radar nowcasting of cloud-to-ground lightning over Houston, Texas. *Wea. Forecasting*, **26**, 199–212, https://doi.org/10.1175/2010WAF2222431.1.

Petersen, W. A., H. J. Christian, and S. A. Rutledge, 2005: TRMM observations of the global relationship between ice water content and lightning. *Geophys. Res. Lett.*, **32**, L14819, https://doi.org/10.1029/2005GL023236.

Rudlosky, S. D., and H. E. Fuelberg, 2010: Pre- and postupgrade distributions of NLDN reported cloud-to-ground lightning characteristics in the contiguous United States. *Mon. Wea. Rev.*, **138**, 3623–3633, https://doi.org/10.1175/2010MWR3283.1.

Saunders, C. P. R., H. Bax-Norman, C. Emerisic, E. E. Avila, and N. E. Castellano, 2006: Laboratory studies of the effect of cloud conditions on graupel/crystal charge transfer in thunderstorm electrification. *Quart. J. Roy. Meteor. Soc.*, **132**, 2653–2673, https://doi.org/10.1256/qj.05.218.

Schmit, T. J., M. M. Gunshor, W. P. Menzel, J. J. Gurka, J. Li, and A. S. Bachmeier, 2005: Introducing the next-generation Advanced Baseline Imager on GOES-R. *Bull. Amer. Meteor. Soc.*, **86**, 1079–1096, https://doi.org/10.1175/BAMS-86-8-1079.

Schultz, C. J., G. T. Stano, P. J. Meyer, B. C. Carcione, and T. Barron, 2017: Lightning decision support using VHF total lightning mapping and NLDN cloud-to-ground data in North Alabama. *J. Oper. Meteor.*, **5**, 134–145, https://doi.org/10.15191/nwajom.2017.0511.

Schultz, E. V., G. T. Stano, L. D. Carey, and W. A. Petersen, 2013: Radar applications for nowcasting lightning cessation. *Sixth Conf. on the Meteorological Applications of Lightning Data*, Austin, TX, Amer. Meteor. Soc., 5.2, https://ams.confex.com/ams/93Annual/webprogram/Paper220563.html.

Scott, M., and L. D. Carey, 2014: Investigating the use of dual-polarization radar variables in forecasting lightning initiation. *26th Conf. on Weather Analysis and Forecasting/22nd Conf. on Numerical Weather Prediction*, Atlanta, GA, Amer. Meteor. Soc., 4A.1A, https://ams.confex.com/ams/94Annual/webprogram/Paper236159.html.

Seroka, G. N., R. E. Orville, and C. Schumacher, 2012: Radar nowcasting of total lightning over the Kennedy Space Center. *Wea. Forecasting*, **27**, 189–204, https://doi.org/10.1175/WAF-D-11-00035.1.

Smith, T., and Coauthors, 2016: Multi-Radar Multi-Sensor (MRMS) severe weather and aviation products: Initial operating capabilities. *Bull. Amer. Meteor. Soc.*, **97**, 1617–1630, https://doi.org/10.1175/BAMS-D-14-00173.1.

Takahashi, T., 1978: Riming electrification as a charge generation mechanism in thunderstorms. *J. Atmos. Sci.*, **35**, 1536–1548, https://doi.org/10.1175/1520-0469(1978)035<1536:REAACG>2.0.CO;2.

Tessendorf, S. A., L. J. Miller, K. C. Wiens, and S. A. Rutledge, 2005: The 29 June supercell observed during STEPS. Part I: Kinematics and microphysics. *J. Atmos. Sci.*, **62**, 4127–4150, https://doi.org/10.1175/JAS3585.1.

Vincent, B. R., L. D. Carey, D. Schneider, K. Keeter, and R. Gonski, 2003: Using WSR-88D reflectivity for the prediction of cloud-to-ground lightning: A central North Carolina study. *Natl. Wea. Dig.*, **27** (1), 35–44.

Wolf, P., 2007: Anticipating the initiation, cessation, and frequency of cloud-to-ground lightning, utilizing WSR-88D reflectivity data. *NWA Electron. J. Oper. Meteor.*, 2007-EJ1, http://nwafiles.nwas.org/ej/pdf/2007-EJ1.pdf.

Woodard, C. J., L. D. Carey, W. A. Petersen, and W. P. Roeder, 2012: Operational utility of dual-polarization variables in lightning initiation forecasting. *Electron. J. Oper. Meteor.*, **13**, 79–102, http://nwafiles.nwas.org/ej/pdf/2012-EJ6.pdf.

Zavodsky, B. T., A. L. Molthan, and M. J. Folmer, 2013: Multispectral imagery for detecting stratospheric air intrusions associated with mid-latitude cyclones. *J. Oper. Meteor.*, **1**, 71–83, https://doi.org/10.15191/nwajom.2013.0107.

Zipser, E. J., and K. Lutz, 1994: The vertical profile of radar reflectivity of convective cells: A strong indicator of storm intensity and lightning probability? *Mon. Wea. Rev.*, **122**, 1751–1759, https://doi.org/10.1175/1520-0493(1994)122<1751:TVPORR>2.0.CO;2.